Advanced Steel Construction – Vol. 17 No. 1 (2021) 66–72
DOI:10.18057/IJASC.2021.17.1.8

BEHAVIOUR OF REINFORCED JOINTS BETWEEN STEEL BEAM AND L-SHAPED WIDE LIMB COMPOSITE COLUMN

Rong-Quan Ma [1], Ping-Yu Zhao [2], Hui-Yong Ban [2, *], Yuan-Qing Wang [2], Yu-Zheng Zhao [3] and Cheng-Bo Peng [4]

[1] *College of Civil Engineering, Tongji University, Shanghai, China*
[2] *Key Laboratory of Civil Engineering Safety and Durability of China Education Ministry, Department of Civil Engineering, Tsinghua University, Beijing, China*
[3] *Beijing Tianheng Construction Group Co. Ltd, Beijing, China*
[4] *China Construction Eight Engineering Division Steel Structure Engineering Company, Shanghai, China*
** (Corresponding author: E-mail: banhy@tsinghua.edu.cn)*

ABSTRACT

Specially-shaped composite columns have attracted more and more attention from either industry or academia, due to their benefits for improving efficiency of use and design of indoor space. This paper presents a research programme on the seismic behaviour of an innovative joint between steel beam and L-shaped wide limb composite column (LSWL-CC). Two full-scale cyclic loading tests are introduced, with failure modes, cyclic behaviour, ultimate capacities, rotation performance, ductility, and energy dissipation being clarified. By using SolidWorks, a parametric model of the joints between steel beams and LSWL-CCs is established, and effects of various parameters are analysed by finite element (FE) analyses through ABAQUS. The FE model is validated against the test results. Furthermore, effects of geometry of the RVPs and the column axial compression ratio on the stiffness, bearing capacity, plastic zone and ductility of the joints are analysed. It is found that, triangular RVPs can make the joints possess similar seismic performance compared with the specimens using trapezoid RVPs. It is suggested to locate the RVPs within the width of the flange in case of the beams and columns having identical width. In addition, optimised geometry of the RVPs with a curved edge may lead to better deformation performance for the joints. Specifically, length of the RVP is suggested to be 1.0~1.2 times height of the beam, its height shall be 1/4 ~ 1/3 of the steel beam height, and its thickness shall be 1.2 times that of the beam flange. The research outcomes may provide valuable information for further research on structures with the L-shaped columns and the joints, and may promote their practical application.

ARTICLE HISTORY

Received: 25 February 2020
Revised: 10 November 2020
Accepted: 10 November 2020

KEYWORDS

Beam-to-column joints;
L-shaped wide limb composite columns;
Reinforcing vertical plate;
Experimental study;
Finite element analysis;
Seismic performance

1. Introduction

Rectangular cross-section columns are widely applied in steel residential building structures, such as concrete-filled steel tube (CFST) ones (Lee *et al*. 2011, Jamaluddin *et al*. 2013, Patel *et al*. 2016, 2019)[1~4], of which the width is normally larger than the thickness of walls, and therefore extended corners are resulted and may reduce indoor space. Use of specially-shaped reinforced concrete columns (Xue *et al*. 2017)[5] and composite columns, such as L-shaped, T-shaped and cross section ones, are adequate for solving this problem due to their benefits in efficient use and design of indoor space (Liu *et al*. 2019)[6]. However, because of their particular geometric properties, innovative beam-to-column joints with improved configurations are required for practical engineering.

Previously, extensive research has been focused on the behaviour of specially-shaped composite columns only, including the static behaviour under compression of L-shaped ones (Chen and Shen 2010, Liu *et al*. 2018, 2019, Rong *et al*. 2017, Xiong *et al*. 2017, Zhang *et al*. 2018, Zhou *et al*. 2015, 2016) [6~13], of T-shaped ones (Liu *et al*. 2018, Rong *et al*. 2016, Tu *et al*. 2014, Wang and Chang 2013, Yang *et al*. 2010, 2015)[8,14~19] and of other types (Wu *et al*. 2017)[20], as well as their dynamic performance (Liu *et al*. 2018, Shen *et al*. 2013, Tu *et al*. 2014, Zhou *et al*. 2012)[14,21~23]. Extensive experimental investigations were conducted, with effects of various configurations of stiffeners, geometry and material strengths being elucidated, and design guidance or prediction formulae were proposed accordingly. In addition, Zhou *et al*. (2015)[24] and Zhang *et al*. (2018)[25] experimentally investigated seismic behaviour of frames with L-shaped composite columns, in which effects of axial compression ratio and beam-to-column stiffness ratios on seismic behaviour of the frames were clarified and the failure mechanism was discussed.

Regarding research on beam-to-column joints, previous work is mainly focusing on that with conventional circular or square CFST columns, including the joints with external diaphragms (Chen and Chung 2003, Li and Han 2011, Rezaifar and Younesi 2017)[26~28], that with bolted connections (Lee *et al*. 2012, Tao *et al*. 2017, Thai *et al*. 2017)[29~31] and with other configurations (Stephens *et al*. 2016)[32]. Investigations on beam-to-column joints fabricated with the specially-shaped composite columns are rather limited. Du *et al*. (2012)[33] experimentally investigated frame joints with T-shaped CFST columns and steel beams as well as exterior diaphragms, and found that increase of width or overhanging length of the stiffening ring may improve the ductility of the joints. Xu *et al*. (2012)[34] tested three frame joints with crisscross CFST columns and steel beams under cyclic loadings, and clarified their failure mechanism as well as effects of axial compression ratios. Liu *et al*. (2016)[35] tested six steel reinforced concrete special-shaped column-beam joints on their seismic behaviour. Liu *et al*. (2017)[36] tested four joints under cyclic loadings, and exterior diaphragm and vertical ribs were utilised in two groups, respectively. Both cross-shaped and T-shaped CFST columns were incorporated. Their effects on the seismic behaviour of the joints were elucidated and design equations for predicting the shear resistance were developed. Zhang *et al*. (2018)[37,38] introduced an innovative joint between L-shaped composite columns and steel beams by employing vertical stiffeners, and tested their cyclic performance. Based on the test results, a simplified trilinear model was proposed for predicting the shear strength versus shear deformation responses as well as a design method being introduced. Zeng *et al*. (2019)[39] investigated experimentally a reduced-scale frame structure with concrete encased L-shaped steel section columns and steel beams on its seismic performance.

Diaphragms are commonly utilised for connecting tubular columns including CFST ones with steel beams. However, use of inner diaphragms may result in challenges for fabrication because it is difficult to be welded along the four edges inside the tubes; the exterior diaphragm is wider than the steel beams and needs more indoor space, and therefore it is inadequate for the specially-shaped columns. An innovative type of beam-to-column joints with reinforcing vertical plates (RVPs) was presented herein for practical use of L-shaped wide-limb composite columns (LSWL-CCs), which are expected to shift the beam plastic hinges but not to increase width of the beam. An experimental programme on the joints was carried out to clarify their seismic performance, and numerical analyses were subsequently conducted with extensive range of parameters being involved. The research outcomes are helpful for understanding the mechanical responses of the reinforced joints, and may provide references for their engineering application.

2. Experimental research

2.1. Test programme

An experimental programme including two full-scale joint specimens were carried out previously by the authors (Ma *et al*. 2017)[40], one with a lattice type

of LSWL-CC (labelled as specimen I) and the other one with a solid type of LSWL-CC (labelled as specimen II). Their general configuration details are illustrated in Figs. 1 and 2, respectively. The composite column of the specimen I is composed of three square CFSTs as boundary elements and diagonal steel-tube (ST) bracings, and that of the specimen II is composed of three square CFSTs as boundary elements as well and double steel plate composite walls. In the composite walls, thickness of the outside steel plate is 12 mm while thickness of the inner stiffener plate is 8 mm. Hot-rolled H-shaped profile HN600×200×11×17 was used to fabricate the steel beam, and two RVPs are attached on both sides of the beam end through welding, respectively, of which thickness is 25 mm. It should be noted that the RVP of specimen I is a cut-corner plate, and that of specimen II is optimized to be a wedge for reducing potential stress concentration. The RVPs should be welded on the beam in factory to ensure the welding quality. Other geometric dimensions can be found in Figs. 1 and 2.

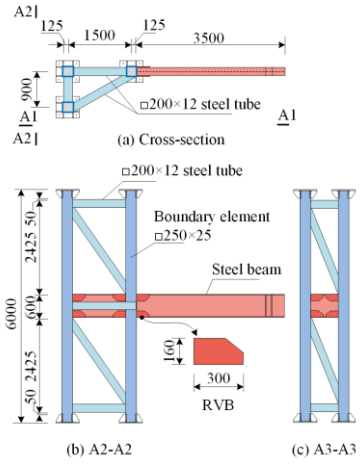

Fig. 1 Geometry of specimen I (Unit: mm)

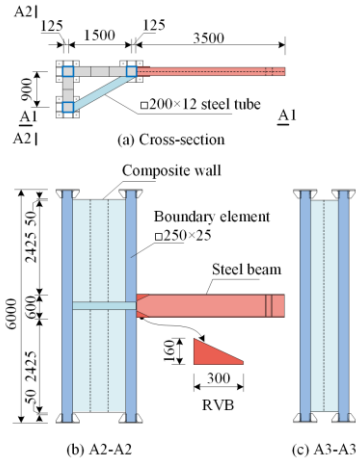

Fig. 2 Geometry of specimen II (Unit: mm)

The tubes in the boundary elements are fabricated from Q420C steel, and other steel components of the specimens are fabricated from Q345C steel. Material properties of the steel are given in Table 1, where the yield strength, the ultimate tensile stress and the elongation percentage after fracture of the steel plates are presented as f_y, f_u and A_{fr}, respectively. The boundary elements and the composite wall of specimen II are filled with concrete, of which equivalent compressive strength f_c is 39.6 MPa on average.

Table 1
Material properties of steel

Grade	Thickness (mm)	f_y (MPa)	f_u (MPa)	A_{fr}
Q420C	25	454.4	606.96	0.25
Q345C	25	358.1	517.8	0.30
	17	360.1	541.4	0.29
	12 (solid wall)	352.1	505.9	0.33
	12 (ST bracing)	390.5	519.3	0.29
	11	368.2	536.9	0.29
	8	352.8	520.7	0.33

The test setup is shown in Fig. 3. Axial compressive force was applied at top of the boundary elements firstly and kept constant, and cyclic loads were applied vertically at the end of the beam, which was laterally braced to prevent lateral-torsional buckling. The axial compressive force applied was 11324.8 kN with a compression ratio of being 0.6. The cyclic loading downward is denoted as "+" and upward as "-".

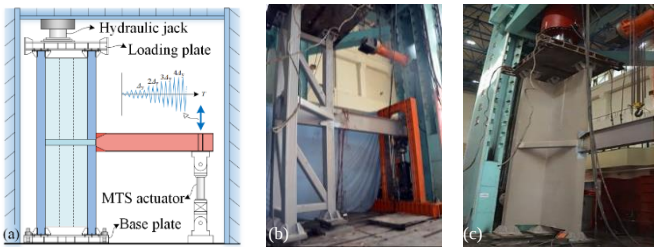

Fig. 3 Test setup: (a) illustration; (b) photo of specimen I (Ma *et al*. 2017[40]); (c) photo of specimen II (Ma *et al*. 2017[40])

Layout of measurement for the two specimens is shown in Fig. 4. The vertical linear variable displacement transformer (LVDT) D1 is used to measure the beam end deflection δ_1. LVDTs D2 and D3 are placed diagonally to measure the panel zone's deformation (δ_2 and δ_3). LVDTs D4 and D5 are used to measure the horizontal displacements δ_4 and δ_5 of the columns. LVDTs D6 and D7 are used to measure the shear deformation δ_6 and δ_7 of the zone of the RVPs. LVDTs D8 and D9 are used to measure the rigid body motion through readings δ_8 and δ_9. Strain gauges are arranged at the location where plastic hinge is expected to develop.

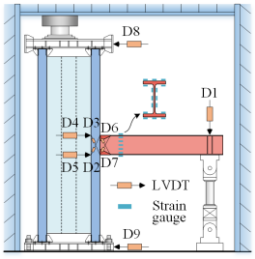

Fig. 4 Layout of measurement

2.2. Test results and analyses

Fig. 5 shows typical failure modes of the specimen I. With an increase of the cyclic loading levels, the beam flange adjacent to the RVPs buckled locally firstly, and then crack was observed within the flange. No visible deformation was identified in the LSWL-CC and the RVPs during the whole loading process. Similar failure modes were found for the specimen II, as shown in Fig. 6.

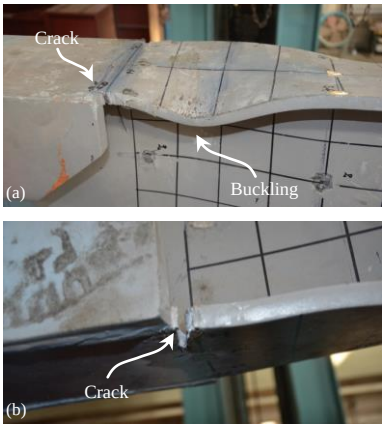

Fig. 5 Failure modes of specimen I: (a) local bucking and crack of top flange; (b) crack at bottom flange

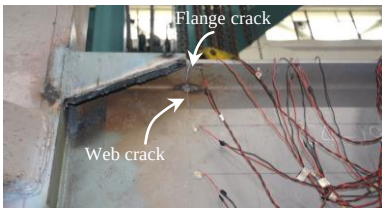

Fig. 6 Failure modes of specimen II

Cyclic loading versus deformation responses were obtained from test results, as shown in Fig. 7. It can be found that both specimens' exhibit a plump shape. Strength degradation was resulted from buckling or initiation of crack within the beam flanges. Plastic hinge within the beam can be developed out of region of the RVPs, and the maximum ratios M/M_p of specimens I and II are 1.13 and 1.10, respectively, in which M_p is the full plastic moment capacity of the plastic hinge and is calculated as being 1031 kN·m from the measured material properties in Table 1. However, development of the plastic deformation of the joints is still insufficient because of their brittle fracture. Based on the cyclic curves and corresponding envelop curves, characterised results including moments M_y, M_u and rotations θ_y, θ_u as well as initial elastic stiffness K_e are summarised in Table 2.

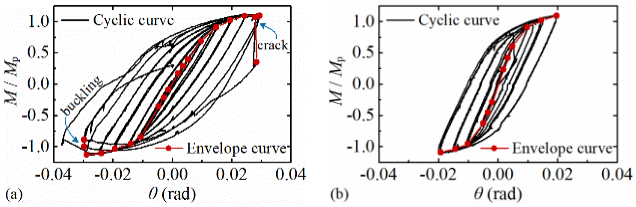

Fig. 7 Cyclic and envelope curves: (a) specimen I; (b) specimen II

Table 2
Characterised results from envelope curves (Ma *et al*. 2017)[40]

Specimen	Load direction	Yield point		Ultimate point		K_e (kN/mm)
		M_y (kN·m)	θ_y (rad)	M_u (kN·m)	θ_u (rad)	
Specimen I	-	-1026	-0.01	-1165	-0.03	8.87
	+	992	0.01	1150	0.03	
Specimen II	-	-881	-0.009	-1124	-0.02	15.72
	+	834	0.008	1127	0.02	

Based on the displacement measurements, the total beam end rotation θ (Hu *et al*. 2014)[41], rotation of the panel zone of beam-to-column joints θ_{pz} (Shi *et al*. 2012)[42], rotation of column θ_c as well as beam rotation θ_b can be derived. Contribution of each rotation component to the total beam end rotation in the last cycle at each loading level is shown in Fig. 8. It can be found that the beam rotation (θ_b) is dominant for both specimens I and II. The maximum rotation of panel zone is about 1.8% and 1.0% of the total beam end rotation, respectively, for specimens I and II. Generally, the results indicate that the rotation capacity of specimen I was greater than that of specimen II. Table 3 gives results of displacement ductility ratio (μ_Δ) and equivalent viscous damping coefficient h_e.

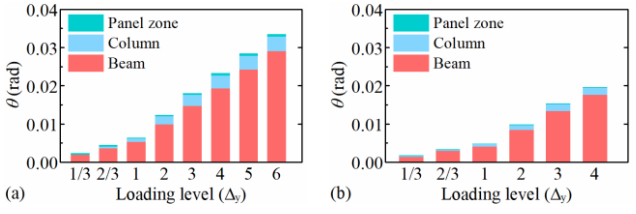

Fig. 8 Contribution of beam end rotation: (a) specimen I; (b) specimen II

Table 3
Ductility and energy dissipation results (Ma *et al*. 2017)[40]

Specimen	Load direction	μ_Δ	$\mu_{\Delta,ave}$	h_e
Specimen I	-	2.45	2.38	0.267
	+	2.38		
Specimen II	-	2.25	2.33	0.264
	+	2.40		

3. Finite Element Modelling and Validation

Based on the previous experimental research programme, a three-dimensional finite element (FE) model of the joints was developed by using ABAQUS, as shown in Fig. 9. A bilinear stress-strain relation was employed to describe the uniaxial one of the steel, and the kinematic hardening model provided by ABAQUS was applied for the steel; the concrete damaged plasticity model was used for the concrete material. Material properties were determined based on the material test results. The Q420 steel tubes and concrete components were meshed by using C3D8R element, and the other steel components including the tubes in the joint zone were meshed through C3D10 element. The steel tube of the column and the steel beam as well as steel plates in the composite wall were tied together for simulating the welds. Hard contact relation between the steel tube and the in-filled concrete was defined, with a friction coefficient of 0.2 being adopted. Either the axial compression load at the top of the composite column or the cyclic loads at the beam end were applied on a reference point defined at the corresponding load surface. The column base was fixed and horizontal displacement of the column top was restrained. Lateral bracing supports were applied to the beam end. The loading process was identical to that in the experiment. Both material and geometric non-linearities were incorporated herein.

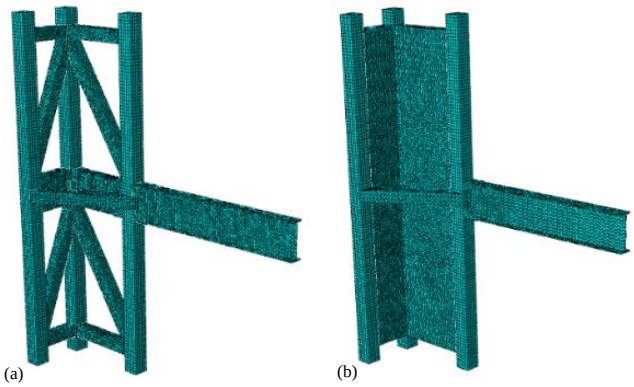

Fig. 9 Mesh of FE models: (a) specimen I; (b) specimen II

Based on the numerical analyses results, cyclic and envelop curves of the load versus displacement responses at the beam end for the two specimens were obtained, and were compared with the test results, as shown in Figs. 10 and 11, respectively. It can be found from the two figures that good agreement in general can be observed between the FE analyses and test results. The cyclic curves obtained from the FE analyses results are basically symmetric between the positive and negative directions, whilst the test curves are not; this is mainly resulted from cracks observed in the tension component during the test. The peak loads in the FE analyses results are close to that of the test results, but the unloading slope in the test curves is slightly lower due to existence of severe cracks. In summary, the FE model developed herein is demonstrated to be adequate for simulating the cyclic behaviour of the specific joints between steel beam and LSWW-CC, and therefore is adopted for further numerical analyses with extended parameters being considered.

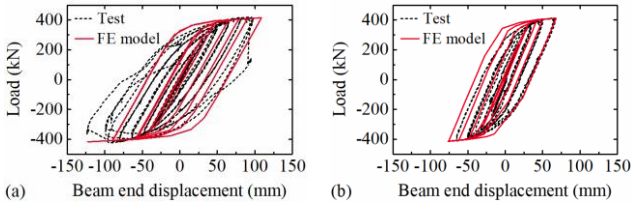

Fig. 20 Comparison of cyclic curves between FE modelling and test results: (a) specimen I; (b) specimen II

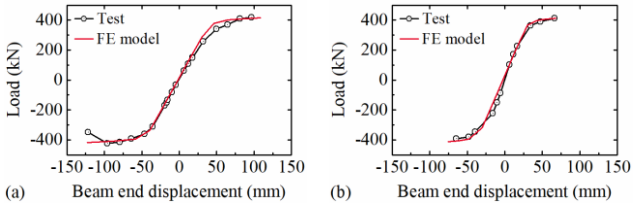

Fig. 11 Comparison of envelope curves between FE modelling and test results: (a) specimen I; (b) specimen II

4. Parametric analyses

4.1. Effects of the RVPs

To clarify effects of the RVPs on the seismic performance of the joints for LSWL-CCs, seismic behaviour of two joints were simulated by using the validated FE modelling approach, including the test specimen (labelled as CONT) as a control group, and another model with identical geometry but without RVPs. Based on the FE analysis results, their cyclic and envelop curves were obtained and are shown in Figs. 12 and 13, respectively, and Fig. 14 presents their stress distribution in the last loading cycle.

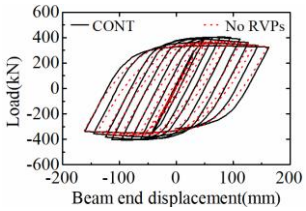

Fig. 32 Comparison of cyclic curves for models with and without RVPs

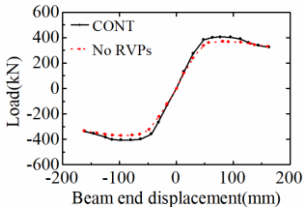

Fig. 13 Comparison of envelope curves for models with and without RVPs

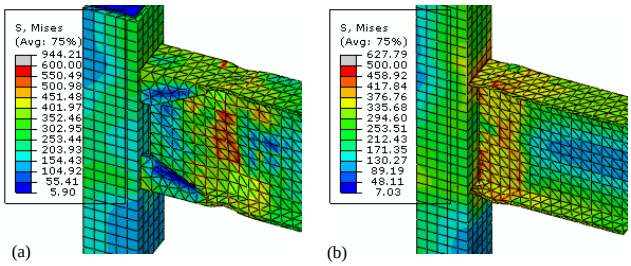

Fig. 14 Stress distribution in the last loading cycle: (a) with RVPs; (b) without RVPs

Based on comparisons in Figs. 12 and 13, it can be found that the joint with RVPs possesses a relatively higher ultimate loading capacity as well as a greater energy dissipation capacity. Meanwhile, from Fig.14, the maximum stress region of the joint without RVPs is closer to the welding zone between column and beam. By applying the RVPs, this maximum stress region has moved away from the welding zone, which is beneficial for preventing brittle failure of the welds.

Consequently, due to the benefits indicated previously in terms of improvement of the mechanical behaviour of the joints and less stress concentration within the welded zone, the RVPs are suggested in practice.

4.2. Dimensions of the RVPs

With the aim of clarifying effects of geometry of the RVPs (as illustrated in Fig. 15) on the seismic performance of the joints for LSWL-CCs developed herein, an extensive range of parametric analyses were conducted. Various values of length a, width b and thickness t of the flange-side RVPs were incorporated, and reasonable geometric dimensions are suggested for design guidance. Given that the deformation of the panel zone is very slight according to the test results, the FE models in the parametric analyses only consider that beam and boundary CFST element to focus on the beam-to-column joint. Failure of the joint in the FE analyses is determined as the case when its loading capacity decreases by 15%.

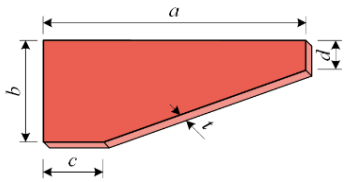

Fig. 45 Geometry of flange-side RVP

i) Effects of length of RVPs

To clarify effects of length of the RVPs on the seismic performance of the joint, five FE models including the test specimen (labelled as CONT) as a control group, were developed, and geometric parameters of the RVPs are given in Table 4, in which H is cross-sectional height of the steel beam, and t_f is thickness of the flange of the steel beam. Geometric dimensions of other components in the FE models are identical to that of the specimen. Based on the FE analyses results, their cyclic and envelop curves are obtained and are shown in Figs. 16 and 17, respectively, and other characteristic results are listed in Table 5.

Table 4
Geometric parameters of FE models with various lengths of RVPs

FE model	Length a (mm)	Width b (mm)	Thickness t (mm)	c (mm)	d (mm)
CONT	0.5H	1/4H	1.5t_f	50	20
L-1	0.75H	1/4H	1.5t_f	50	20
L-2	H	1/4H	1.5t_f	50	20
L-3	1.2H	1/4H	1.5t_f	50	20
L-4	1.5H	1/4H	1.5t_f	50	20

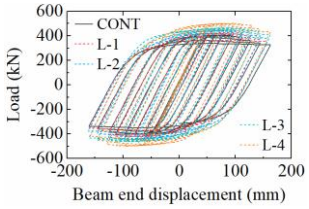

Fig. 56 Comparison of cyclic curves for models with different lengths of RVPs

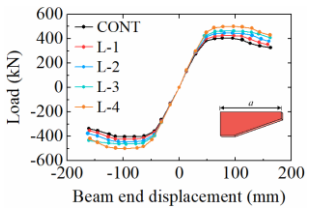

Fig. 17 Comparison of envelope curves for models with different lengths of RVPs

Table 5
Characteristic results of FE models with various lengths of RVPs

FE model	Loading direction	Ultimate bearing capacity (kN)	Yield displacement Δ_y (mm)	Ultimate displacement Δ_u (mm)	Ductility coefficient μ
CONT	Neg.	-404.92	-44.01	-145.31	3.30
	Pos.	404.95	48.15	144.00	2.99
L-1	Neg.	-424.58	-44.01	-145.49	3.31
	Pos.	424.79	48.68	142.84	2.93
L-2	Neg.	-446.20	-44.01	-162.93	3.70
	Pos.	445.90	48.68	160.14	3.29

L-3	Neg.	-463.92	-44.01	-161.00	3.66
	Pos.	463.73	44.98	162.59	3.61
L-4	Neg.	-499.95	-48.42	-159.27	3.29
	Pos.	499.84	48.37	162.26	3.35

The FE analyses results indicate that the cyclic curves of all the five models are plump, representing their good energy dissipation capacity. With an increase in the length of the RVPs, the loading capacity of the joints increase significantly from 405 kN of the model CONT to 500 kN of the model L-4. The five models all exhibite good deformation ability, and it can be seen from Table 5 that when the length of the RVPs is 1.0 ~ 1.2 times of the cross-sectional height of the steel beam, the ductility coefficient is the largest, and this range for the length is recommended for practical usage.

ii) Effects of width of RVPs

To evaluate effects of width of the RVPs on the cyclic performance of the joint, four FE models including the test specimen (labelled as CONT) as a control group were developed, of which values of the geometric parameters are given in Table 6. Based on the FE analyses results, their cyclic and envelope curves are obtained and plotted in Figs. 18 and 19, respectively, and other characteristic properties are listed in Table 7.

Table 6
Geometric parameters of FE models with various widths of RVPs

FE model	Length a (mm)	Width b (mm)	Thickness t (mm)	c (mm)	d (mm)
CONT	0.5H	1/4H	1.5t_f	50	20
W-1	0.5H	1/3H	1.5t_f	50	20
W-2	0.5H	1/5H	1.5t_f	50	20
W-3	0.5H	1/8H	1.5t_f	50	20

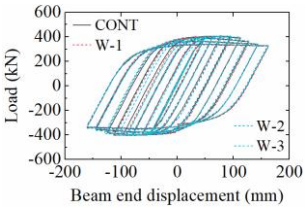

Fig. 68 Comparison of cyclic curves for models with different widths of RVPs

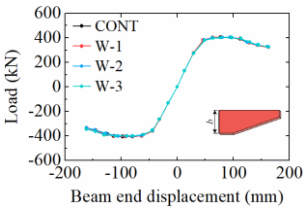

Fig. 19 Comparison of envelope curves for models with different widths of RVPs

Table 7
Characteristic results of FE models with various widths of RVPs

FE model	Loading direction	Ultimate bearing capacity (kN)	Yield displacement Δ_y (mm)	Ultimate displacement Δ_u (mm)	Ductility coefficient μ
CONT	Neg.	-404.92	-44.01	-145.31	3.30
	Pos.	404.95	48.15	144.00	2.99
W-1	Neg.	-405.46	-44.01	-146.23	3.32
	Pos.	405.58	47.26	142.50	3.02
W-2	Neg.	-404.21	-44.01	-146.44	3.33
	Pos.	404.07	48.68	143.81	2.95
W-3	Neg.	-400.42	-44.01	-145.61	3.31
	Pos.	400.82	48.71	143.50	2.95

Based on the FE analysis results, it can be found that the cyclic curves of all the four FE models are plump without any visible differences, indicating their good energy dissipation capacities as well as limited effects of variation in the width of the RVPs. Difference of the loading capacities of all the four models is lower than 1% generally. In case of the width being 1/8 of the cross-sectional height of the steel beam, the loading capacity is the lowest, and therefore a width no less than 1/5 of the beam height is recommended for practice. All the four models possessed good deformation ability and similar ductility coefficients.

iii) Effects of thickness of RVPs

To understand effects of thickness of the RVPs on the seismic performance of the joints, five models including the test specimen (labelled as CONT) as the control group were developed, and their geometric parameters are listed in Table 8. Based on the FE analysis results, their cyclic and envelope curves with various thicknesses of the RVPs are shown in Figs. 20 and 21, respectively, and other characteristic properties are given in Table 9.

Table 8
Geometric parameters of FE models with various thickness of RVPs

FE model	Length a (mm)	Width b (mm)	Thickness t (mm)	c (mm)	d (mm)
CONT	0.5H	1/4H	1.5t_f	50	20
T-1	0.5H	1/4H	1.2t_f	50	20
T-2	0.5H	1/4H	1.0t_f	50	20
T-3	0.5H	1/4H	0.8t_f	50	20
T-4	0.5H	1/4H	0.5t_f	50	20

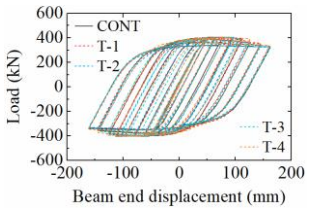

Fig. 20 Comparison of cyclic curves for models with different thickness of RVPs

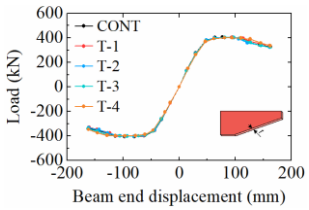

Fig. 21 Comparison of envelope curves for models with different thickness of RVPs

Table 9
Characteristic results of FE models with various widths of RVPs

FE model	Loading direction	Ultimate bearing capacity (kN)	Yield displacement Δ_y (mm)	Ultimate displacement Δ_u (mm)	Ductility coefficient μ
CONT	Neg.	-404.92	-44.01	-145.31	3.30
	Pos.	404.95	48.15	144.00	2.99
T-1	Neg.	-403.82	-44.01	-146.29	3.32
	Pos.	404.19	48.68	145.62	2.99
T-2	Neg.	-402.78	-44.01	-142.68	3.24
	Pos.	403.08	48.68	145.50	2.99
T-3	Neg.	-402.28	-46.32	-146.50	3.16
	Pos.	401.86	47.37	145.00	3.06
T-4	Neg.	-399.57	-46.57	-148.50	3.19
	Pos.	399.52	46.97	145.51	3.10

Based on the FE analysis results it is indicated that, all the five models exhibit good energy dissipation capacities because of their plump cyclic curves. With a decrease of the RVP thickness, their loading capacities decrease generally from 405 kN for the model CONT to 399.52 kN for the model T-4.

All the five models possess good deformation ability, and their ductility coefficients are generally constant. In practice, the thickness of the RVPs is recommended to be no less than half of the flange thickness of the steel beam.

4.2. Optimisation of the RVPs

In order to reduce the unfavourable effects of stress concentration on the mechanical behaviour of the joints and to prevent facture, both geometry and location of the RVPs are optimised. The cut corner one that is applied in specimen I as shown in Fig. 22(a), is firstly optimised to the wedge one as shown in Fig. 22(b), and then it is further moved towards the web, i.e. its vertical outside surface is flush with the toe of the beam flange as shown in Fig. 22(c).

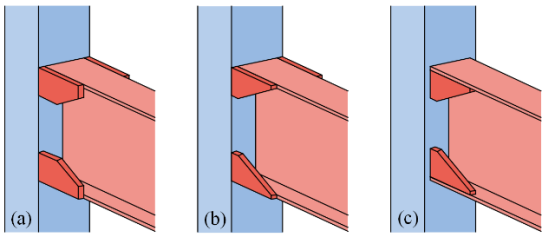

Fig. 22 Optimisation of RVPs: (a) cut corner one; (b) wedge one; (c) flush wedge one

FE models are established for the three types of joints, to which an identical loading spectrum is applied for comparison of their loading responses. Based on the FE analysis results, Figs. 23 and 24 present their stress distribution at the same loading level in elastic and inelastic ranges, respectively. Their load versus displacement curves are shown in Fig. 25.

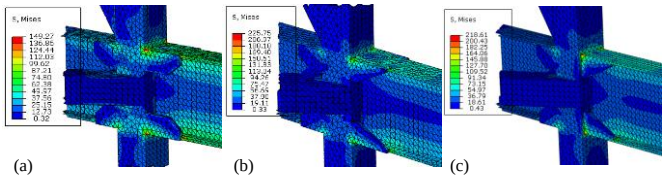

Fig. 23 Stress distribution in elastic state: (a) cut corner RVPs; (b) wedge RVPs; (c) flush wedge RVPs

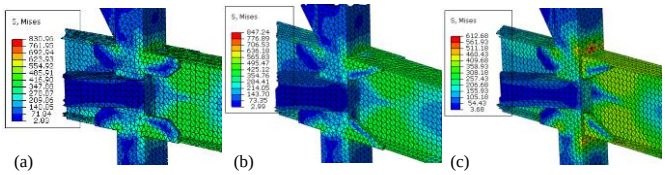

Fig. 24 Stress distribution in inelastic state: (a) cut corner RVPs; (b) wedge RVPs; (c) flush wedge RVPs

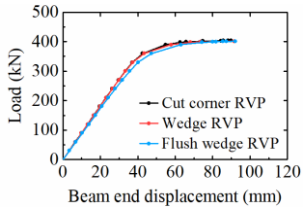

Fig. 25 Load-displacement curves of the joints with RVPs varying in geometry

Based on Figs. 23~25, it can be found that the joint with flush wedge RVPs possesses the lowest level of stress concentration, because its maximum stress magnitude is significantly less than the others', particularly in the inelastic range. With respect to the load versus displacement curves as shown in Fig. 25, no visible difference is observed between the two joints with cut corner and wedge RVPs; whilst for the joint with flush wedge RVPs, its initial stiffness is lower than the other two by 5% approximately. Ultimate bearing capacities of the three joints are basically the same.

Consequently, due to the benefits indicated previously for the use of the flush wedge RVPs in terms of reduction of the stress concentration but limited effects on the loading capacity and stiffness, the configuration details of the joints with the flush wedge RVPs are recommended in practice.

To further optimise the geometry of the RVP for reducing stress concentration, the cut corner RVP was modified into a plate with an arc edge, as shown in Fig. 26. Cyclic behaviour of another joint was simulated through the FE model, which applied the arc-edge RVPs; other parameters of the joint are kept the same as previous ones. Based on the FE analysis results, its cyclic and envelope curves are obtained and are compared with that of joints with cut corner RVPs in Figs. 27 and 28, respectively. Table 10 lists other characteristic mechanical properties.

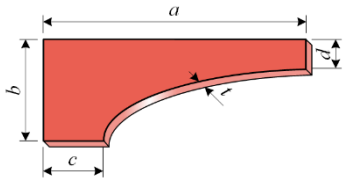

Fig. 26 Geometry of flange-side arc-edge RVP

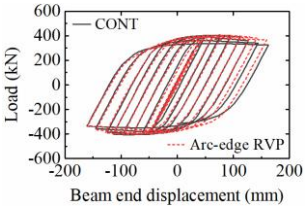

Fig. 27 Comparison of cyclic curves for models with cut corner and arc-edge RVPs

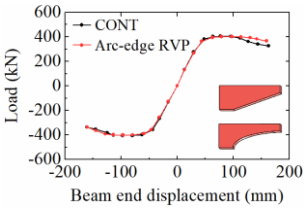

Fig. 28 Comparison of envelope curves for models with cut corner and arc-edge RVPs

Table 10
Characteristic results of FE models with cut corner and arc-edge RVPs

FE model	Loading direction	Ultimate bearing capacity (kN)	Yield displacement Δ_y (mm)	Ultimate displacement Δ_u (mm)	Ductility coefficient μ
BASE	Neg.	-404.92	-44.01	-145.31	3.30
	Pos.	404.95	48.15	144.00	2.99
ARC-PLATE	Neg.	-400.20	-46.32	-160.27	3.46
	Pos.	401.67	43.60	159.48	3.66

It can be found that the cyclic curves of the two models are both plump, indicating their good energy dissipation capacity. The loading capacity of the joint with arc-edge RVPs is slightly lower than that of the other one. Both of them have good deformation ability; specifically, the ductility coefficient as well as the deformation ability of the joint with the arc-edge RVPs is slightly higher than that of the other, due to its reduced stress concentration.

5. Conclusions

Two full-scale steel beam-to-LSWW-CCs joints were tested to evaluate their seismic performance, and FE models were developed accordingly and further validated against the test results. Through an extensive range of parametric analyses, effects of geometry of the RVPs were clarified, and optimised shapes of the RVPs was proposed. Based on the research work presented herein, some conclusions are made as follows.

- The two specimens both fail due to cracks within the beam flange adjacent to the RVPs. Plastic hinge of this type of joint moves to the beam section adjacent to the RVPs as expected. The loading capacities of the two specimens are close to each other approximately and exceed the plastic moment capacity; rotations of the beam and column contribute the most to the total beam end rotation, and that of the panel zone can be neglected.
- Use of the RVPs may increase the loading and energy dissipation capacity,

and reduced the stress concentration within the welded zone between the column and beam.

- The length of the RVPs possesses significant effects on the seismic performance of the joints, and with an increase of the length, the loading capacity increases and the ductility is generally constant. Effects of the width and the thickness of the RVP on seismic behaviour of the joints are insignificant.
- Based on the parametric analyses, it is recommended that the length of the RVP shall be 1.0~1.2 times the cross-sectional height of the steel beam, its width shall be no less than 1/5 of the beam height, and its thickness shall be no less than half of the thickness of the beam flange.
- The cut corner RVP may be optimised into a wedge one without visible loose of either loading capacity or stiffness but with economic benefits in terms of less use of steel. Besides, by moving the RVP towards the web of the beam with its surface being flush with the flange toe, the stress concentration may be reduced and potential fracture would become less severe. Besides, use of the arc-edge RVP may also reduce the stress concentration. Both flush wedge and arc-edge RVPs are recommended to be applied in the joints.

The research outcomes may provide valuable reference for practical engineering of such joints and the LSWW-CCs. Despite this, there are still other factors, e.g., steel grade of the RVPs, welding methods of the RVPs, etc., influencing the mechanical performance of such new joint, and further research is needed to verify and improve the design guidance proposed herein.

References

[1] Lee, S.H., Uy, B., Kim, S.H., Choi, Y.H. and Choi, S.M., "Behavior of high-strength circular concrete-filled steel tubular (CFST) column under eccentric loading", *Journal of Constructional Steel Research,* 67(1): 1-13,2011.

[2] Jamaluddin, N., Lam, D., Dai, X.H. and Ye, J., "An experimental study on elliptical concrete filled columns under axial compression", *Journal of Constructional Steel Research,* 87: 6-16,2013.

[3] Patel, V.I., Uy, B., Prajwal, K.A. and Aslani, F., "Confined concrete model of circular, elliptical and octagonal CFST short columns", *Steel and Composite Structures*, 22(3): 497-520,2016.

[4] Patel, V.I., Hassanein, M.F., Thai, H.T., Al Abadi, H., Elchalakani, M. and Bai, Y., "Ultra-high strength circular short CFST columns: Axisymmetric analysis, behaviour and design", *Engineering Structures*, 179: 268-283,2019.

[5] Xue, J.Y., Zhou, C.F. and Liu, Z.Q., "Research on damage of solid-web steel reinforced concrete T-shaped columns subjected to various loadings", *Steel and Composite Structures*, 24(4): 409-423,2017.

[6] Liu, J.P., Song, H. and Yang, Y.L., "Research on mechanical behavior of L-shaped multi-cell concrete-filled steel tubular stub columns under axial compression", *Advances in Structural Engineering*, 22(2): 427-443,2019.

[7] Chen, Z.Y. and Shen, Z.Y., "Behavior of L-shaped concrete-filled steel stub columns under axial loading: Experiment", *Advanced Steel Construction*, 6(2): 688-697,2010.

[8] Liu, X.G., Xu, C.Z., Liu, J.P. and Yang, Y.L., "Research on special-shaped concrete-filled steel tubular columns under axial compression", *Journal of Constructional Steel Research*, 147: 203-223,2018.

[9] Rong, B., Feng, C.X., Zhang, R.Y., You, G.C. and Liu, R., "Compression-bending performance of L-shaped column composed of concrete filled square steel tubes under eccentric compression", *International Journal of Steel Structures*, 17(1): 325-337,2017.

[10] Xiong, Q.Q., Chen, Z.H., Zhang, W., Du, Y.S., Zhou, T. and Kang, J.F., "Compressive behaviour and design of L-shaped columns fabricated using concrete-filled steel tubes", *Engineering Structures*, 152: 758-770,2017.

[11] Zhang, W., Chen, Z.H. and Xiong, Q.Q., "Performance of L-shaped columns comprising concrete-filled steel tubes under axial compression", *Journal of Constructional Steel Research*, 145: 573-590,2018.

[12] Zhou, T., Xu, M.Y., Wang, X.D., Chen, Z.H. and Qin, Y., "Experimental study and parameter analysis of L-shaped composite column under axial loading", *International Journal of Steel Structures*, 15(4):797-807,2015.

[13] Zhou, T., Xu, M.Y., Chen, Z.H., Wang, X.D. and Wang, Y.W., "Eccentric loading behavior of L-shaped columns composed of concrete-filled steel tubes", *Advanced Steel Construction*, 12(3): 227-244,2016.

[14] Liu, J.P., Yang, Y.L., Song, H. and Wang, Y.Y., "Numerical analysis on seismic behaviors of T-shaped concrete-filled steel tubular columns with reinforcement stiffeners", *Advances in Structural Engineering*, 21(9): 1273-1287,2018.

[15] Rong, B., You, G.C., Zhang, R.Y., Feng, C.X. and Liu, R., "Studies on T-shaped composite columns consist of multi separate concrete-filled square tubular steel sections under eccentric axial load", *Steel and Composite Structures*, 22(2): 217-234,2016.

[16] Tu, Y.Q., Shen, Y.F. and Li, P., "Behaviour of multi-cell composite T-shaped concrete-filled steel tubular columns under axial compression", *Thin-Walled Structures*, 85: 57-70,2014.

[17] Wang, Q.T. and Chang, X., "Analysis of concrete-filled steel tubular columns with 'T' shaped cross section (CFTTS)", *Steel and Composite Structures*, 15(1): 41-55,2013.

[18] Yang, Y.L., Yang, H. and Zhang, S.M., "Compressive behavior of T-shaped concrete filled steel tubular columns", *International Journal of Steel Structures*, 10(4): 419-430,2010.

[19] Yang, Y.L., Wang, Y.Y., Fu, F. and Liu, J.C., "Static behaviour of T-shaped concrete-filled steel tubular columns subjected to concentric and eccentric compressive loads", *Thin-Walled Structures*, 95: 374-388,2015.

[20] Wu, H.P., Qiao, Q.Y., Cao, W.L., Dong, H.Y. and Zhang J.W., "Axial compressive behavior of special-shaped concrete filled tube mega column coupled with multiple cavities", *Steel and Composite Structures*, 23(6): 633-646,2017.

[21] Shen, Z.Y., Lei, M., Li, Y.Q., Lin, Z.Y. and Luo, J.H., "Experimental study on seismic behavior of concrete-filled L-shaped steel tube columns", *Advances in Structural Engineering*, 16(7): 1235-1247,2013.

[22] Tu, Y.Q., Shen, Y.F., Zeng, Y.G. and Ma, L.Y., "Hysteretic behaviour of multi-cell T-Shaped concrete-filled steel tubular columns", *Thin-Walled Structures*, 85: 106-116,2014.

[23] Zhou, T., Chen, Z.H. and Liu, H.B., "Seismic behavior of special shaped column composed of concrete filled steel tubes", *Journal of Constructional Steel Research*, 75: 131-141,2012.

[24] Zhou, T., Jia, Y.M., Xu, M.Y., Wang, X.D. and Chen, Z.H., "Experimental study on the seismic performance of L-shaped column composed of concrete-filled steel tubes frame structures", *Journal of Constructional Steel Research*, 114: 77-88,2015.

[25] Zhang, J.C., Li, Y., Zheng, Y. and Wang, Z.J., "Seismic damage investigation of spatial frames with steel beams connected to L-shaped concrete-filled steel tubular (CFST) columns", *Applied Sciences*, 8(10): 1713,2018.

[26] Cheng, C.T. and Chung L.L., "Seismic performance of steel beams to concrete-filled steel tubular column connections", *Journal of Constructional Steel Research*, 59(3): 405-426,2003.

[27] Li, W. and Han, L.H., "Seismic performance of CFST column to steel beam joints with RC slab: Analysis", *Journal of Constructional Steel Research*, 67: 127-139,2011.

[28] Rezaifar, O. and Younesi, A., "Experimental study discussion of the seismic behavior on new types of internal/external stiffeners in rigid beam-to-CFST/HSS column connections", *Construction and Building Materials*, 136: 574-589,2017.

[29] Lee, S.H., Kim, Y.H. and Choi, S.M., "Shear strength formula of CFST column-beam pinned connections", *Steel and Composite Structures*, 13(5): 409-421,2012.

[30] Tao, Z., Li, W., Shi, B.L. and Han, L.H., "Behaviour of bolted end-plate connections to concrete-filled steel columns", *Journal of Constructional Steel Research*, 134: 194-208,2017.

[31] Thai, H.T., Vo, T.P., Nguyen, T.K. and Pham, C.H., "Explicit simulation of bolted endplate composite beam-to-CFST column connections", *Thin-Walled Structures*, 119: 749-759,2017.

[32] Stephens, M.T., Berg, L.M., Lehman, D.E. and Roeder, C.W., "Seismic CFST column-to-precast cap beam connections for accelerated bridge construction", *Journal of Structural Engineering*, 142(9): 04016049,2016.

[33] Du, G.F., Ma, C. and Xu, C.X., "Experimental research on seismic behavior of exterior frame joints with T-Shaped CFST column and steel beam", *Advanced Materials Research*, 368-373: 183-188,2012.

[34] Xu, C.X., Liu, X.Q. and Zhang, J.C., "Experimental research on seismic behavior of spatial joints in a composite frame consisting of CFST crisscross section columns and steel beams", *Proceedings of the Twelfth International Symposium on Structural Engineering*, Wuhan, China, November,2012.

[35] Liu, Z.Q., Xue, J.Y. and Zhao, H.T., "Seismic behavior of steel reinforced concrete special-shaped column-beam joints", *Earthquakes and Structures*, 11(4): 665-680,2016.

[36] Liu, J.C., Yang, Y.L., Liu J.P. and Zhou, X.H. "Experimental investigation of special-shaped concrete-filled steel tubular column to steel beam connections under cyclic loading", *Engineering Structures*, 151: 68-84,2017.

[37] Zhang, W., Chen Z.H., Xiong, Q.Q. and Zhou, T., "Calculation method of shear strength of vertical stiffener connections to L-CFST columns", *Advances in Structural Engineering*, 21(6): 795-808,2018.

[38] Zhang, W., Chen Z.H., Xiong, Q.Q., Zhou, T., Rong, X. and Du, Y.S., "Experimental seismic behaviour of L-CFST column to H-beam connections", *Steel and Composite Structures*, 26(6): 793-808,2018.

[39] Zeng, L., Ren, W.T., Zou Z.T., Chen, Y.G., Xie, W. and Li, X.J., "Experimental study on seismic behavior of frame structures composed of concrete encased columns with L-shaped steel section and steel beams", *Earthquakes and Structures*, 16(1): 97-107,2019.

[40] Ma, R.Q., Ban, H.Y., Zhao, Y.Z., Wang, Y.Q., Li, Q. and Liu, M., "Experimental study on seismic behavior of steel beam to wide-flange specially-shaped composite column connections", *Journal of Building Structures*, 38(6): 105-113,2017. (in Chinese)

[41] Hu F.X., Shi, G., Bai Y. and Shi, Y.J., "Seismic performance of prefabricated steel beam-to-column connections", *Journal of Constructional Steel Research*, 102: 204-216,2014.

[42] Shi, G., Fan, H., Bai, Y., Yuan, F, Shi, Y.J. and Wang, Y.Q., "Improved measure of beam-to-column joint rotation in steel frames", *Journal of Constructional Steel Research*, 70: 298-307,2012.